

Energy-loss enhancement and charge-equilibration time for highly charged xenon ions at near-Bohr velocity in solids

Z. Y. Song ^{1,2,*} Z. W. Wu,^{3,4,5} Z. H. Yang,^{1,†} B. L. Zhang,¹ and G. Q. Xiao^{1,2}

¹*Institute of Modern Physics, Chinese Academy of Sciences, Lanzhou 730000, China*

²*School of Nuclear Science and Technology, University of Chinese Academy of Sciences, Beijing 100049, China*

³*Key Laboratory of Atomic and Molecular Physics & Functional Materials of Gansu Province,*

College of Physics and Electronic Engineering, Northwest Normal University, Lanzhou 730070, China

⁴*Helmholtz-Institut Jena, Fröbelstieg 3, D-07743 Jena, Germany*

⁵*GSI Helmholtzzentrum für Schwerionenforschung GmbH, Planckstrasse 1, D-64291 Darmstadt, Germany*



(Received 26 June 2022; accepted 5 December 2022; published 19 December 2022)

We probe the energy-loss enhancement in preequilibration and the charge-equilibration time for highly charged Xe ions ($q_{\text{in}} = 15\text{--}26$) at near-Bohr velocity impinging on an Al target by measuring the dependence of the Xe L -shell x-ray yield on the initial charge state of the ions. The present results are found to be very consistent with those obtained in ion-transmission thin-foil experiments. The charge-equilibrium time is measured in the near-Bohr velocity region of highly charged ions in solids. Moreover, for the present collision system it is demonstrated by measuring the inner-shell x rays that the ionization of the inner-shell electrons of the projectile ions starts to contribute to ion energy loss at near-Bohr velocity.

DOI: [10.1103/PhysRevA.106.062817](https://doi.org/10.1103/PhysRevA.106.062817)

I. INTRODUCTION

Ion-solid interaction has attracted continuous interest and can be traced back to the beginning of the 20th century [1–3] owing to its great significance not only from a fundamental perspective but also for applications ranging from material [4–7] and plasma [8,9] studies to medical treatment of tumors [10]. As ions move through solid materials, multiple collisions including elastic and inelastic processes result in energy loss of the ions during each of the collisions. The stopping power S , i.e., the energy loss per unit path length, is employed to characterize the ability of materials to stop ions. S depends not only on the parameters of the ions (species, kinetic and potential energies) but also on the target characteristics, which are determined by the sum of elastic energy transfer to the target nucleus S_n and inelastic energy transfer to the target electrons S_e . Accurate knowledge of the stopping power is fundamental to ion-solid interactions and also critical to the formation of nanostructures under irradiation, especially for collisions of highly charged ions with solids since they introduce promising prospects to atomic physics [11–13] and the synthesis of materials with new properties [4–7].

For the collisions of highly charged ions with solids, the power of materials to stop ions is known to be dependent on the charge state of the projectile [14,15]. An equilibration charge state q_{eq} will be reached after ions travel a particular distance called the “charge-state equilibration length” d , as shown schematically in Fig. 1. In the course of the preequilibration stage the stopping power exhibits an enhanced

behavior compared to the case in the equilibration charge state [16–20]. For ions with moderate energies (e.g., 3225 keV to 658 MeV for the ^{129}Xe projectiles used in the present work), Bohr deduced an expression for the equilibration charge state, $q_{\text{eq}} = v/v_o Z^{1/3}$, with v being the ion velocity, v_o being the Bohr velocity, and Z being the projectile atomic number [21]. Later, an improved expression was also presented by fitting a large number of experimental values [22]. By assuming metal target electrons were a Fermi gas, Brandt *et al.* [23] believed that a linear-response mechanism is sufficient to characterize the change in the projectile ion charge state in the preequilibration stage; that is, the projectile charge state approaches the equilibration charge state at a constant rate. Such a linear-response mechanism has been widely used and verified in many subsequent studies [19,24–27].

Although kinetic energy loss of ions traveling through various media has been extensively investigated [8,9,16–20,28–36], some novel experimental phenomena were still found recently. For instance, by using 50–200-keV protons and helium ions transmitting through self-supporting single-crystalline silicon foils, a lower energy loss was observed in channeling geometry than in random geometry [31]. The corresponding energy-loss difference between the two geometries increases with initial kinetic energy for the case of protons, whereas it decreases for the helium ions [31]. In collisions of 100-keV/u helium ions with a hydrogen-discharge plasma, an enhanced energy loss of about 20% was observed [8] compared to the predictions of effective charge models. The enhancement was demonstrated to be caused by the contributions of excited states populated in the collisions, even though their population fraction is less than 10% [8]. Moreover, in collisions of highly charged ions with carbon nanomembranes or a monolayer of graphene [18,19,25–27], strong enhancements of the kinetic

*songzhy@impcas.ac.cn

†z.yang@impcas.ac.cn

energy loss were also found by increasing the initial charge state of the ions.

In order to account for the energy loss of heavy ions in materials, especially for the enhanced energy loss of highly charged ions in the course of the preequilibration stage, several models based on the interaction potential between the ions and solid [20,28,29] have been developed following the progress of experimental research. These models reveal that the charge exchange between the target and the ion influences the scattering potential, which results in a close coupling between nuclear and electronic loss, and consequently, they cannot be treated independently anymore. With the development of numerical calculation methods, it became possible to calculate the stopping power from first principles [32–36]. Up to now, it has been gradually expanded from the ability to calculate the stopping power of light ions such as protons [32,33] in materials to being able to calculate that of heavy ions [34–36] with an explicit account for the electronic structure of both the target and the projectiles. Ullah *et al.* [35] simulated the electronic stopping power in self-irradiated Ni for a wide range of energy within the frame of real-time time-dependent density-functional theory. It was found that the inner-shell electrons, particularly those of the projectile, begin to make a major contribution to the energy dissipation as the projectile velocity increases. Lee *et al.* [36] also found that the core electrons of heavy projectiles can affect the electronic stopping power and thus have an unexpected influence on the charge state of the projectiles.

To the best of our knowledge, there is no direct experimental observation that connects the core-electron excitation or ionization of projectiles with the energy loss of ions. This is primarily because in traditional energy-loss experiments, ion-transmission thin films [16,19,24–27] or the ion-surface scattering method (e.g., Ref. [3] and references therein) are usually employed, and the energy loss is determined by measuring the time of flight of ions. In this paper, we propose to explore the energy loss and the charge-equilibration time of highly charged ions in materials by measuring the characteristic x-ray yield of projectiles and report on the experimental evidence that core-electron ionization of projectiles is, indeed, involved in the energy loss of ions in the near-Bohr velocity region. As shown schematically in Fig. 1, as projectile ions such as Xe^{q+} with near-Bohr velocity enter into the target at an incident angle of 45° , inner-shell (core) electrons of the projectile would be ionized by collisions as long as its kinetic energy is greater than the ionization threshold energies [Fig. 1(a)]. In the case that the initial charge state of the projectile ions is larger than q_{eq} , taking into account the energy-loss enhancement in the preequilibration regime as observed in Refs. [16–20], the ions lose their kinetic energy at a faster rate and reach the equilibration charge state on a femtosecond timescale, and then the energy loss proceeds at the rate of the equilibration state [Fig. 1(b)]. The total inner-shell x-ray yield over this timescale can be expressed approximately as $\sum_i N \sigma_X \Delta x_i$, with N and σ_X being the target atomic density and the x-ray emission cross section, respectively, and Δx_i being the i th increment of depth. As can be seen from Fig. 1(b), the area surrounded by the three points E_0 , E_{th} , and A (or B and C) for collisions at q_{eq} (or q_1 and q_2) reads $\sum_i (E_i - E_{\text{th}}) \Delta x_i$, which is proportional to Δx_i and

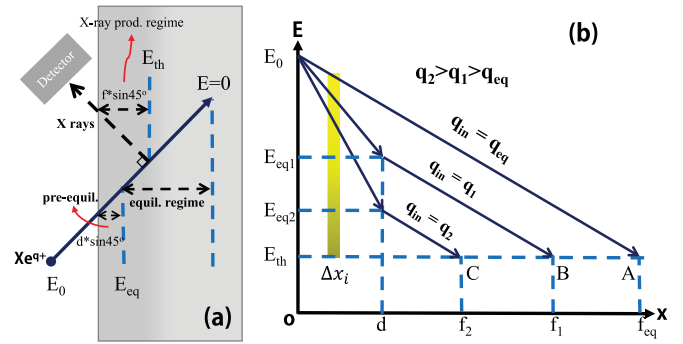


FIG. 1. (a) As the projectile ions $\text{Xe}^{q_{\text{in}}+}$ with initial kinetic energy E_0 enter into the target, inner-shell electrons of the projectile are ionized as long as the kinetic energy is larger than their ionization threshold energy E_{th} , at which the ion depth in the target is f_{eq} (f_1 or f_2) for projectile ions with initial charge state $q_{\text{in}} = q_{\text{eq}}$ (q_1 or q_2). (b) For $q_{\text{in}} > q_{\text{eq}}$, the enhanced stopping power S leads to a steeper decrease of the ion energy in the preequilibration stage compared to the case for $q_{\text{in}} = q_{\text{eq}}$. After equilibration, the ion energy decreases at a constant rate. The total x-ray yield emitted is given approximately by $\sum_i N \sigma_X \Delta x_i$ (N and σ_X represent the target density and the x-ray emission cross section, respectively), which is proportional to the area enclosed by the three points E_0 , E_{th} , and A (or B and C) for initial charge states q_{eq} (or q_1 and q_2) since the area can be expressed as $\sum_i (E_i - E_{\text{th}}) \Delta x_i$.

decreases with the increase of the initial charge state of the ions. Therefore, the x-ray yield will decrease gradually with the increase of the initial charge state of the projectile if its initial kinetic energy remains unchanged.

II. EXPERIMENTS

The present experiment was performed using near-Bohr-velocity ^{129}Xe ions with an initial charge state q_{in} from 15 to 26. The ions were supplied by the permanent-magnet electron-cyclotron-resonance ion resource (ECRIS) at the 320-kV high-voltage platform located at the Institute of Modern Physics of the Chinese Academy of Sciences, Lanzhou. The details of the ECRIS and experimental setup were described elsewhere [37,38]. Briefly, an ion beam with multiple charge states is extracted from the source by an electrode and then selected to be a single-charge-state ion beam by a 90° analyzing magnet. Afterwards, the Xe ion beam with an initial charge state q_{in} is focused by a quadrupole, collimated by two sets of four jaw slits, and, finally, delivered into the ultrahigh-vacuum target chamber to bombard the Al target at 45° . The diameter of the ion beam spot on the target is about 2 mm, and the beam intensity is on the order of nanoamperes. The target used in the experiment has a polished surface, a purity of 99.99%, an area of $20 \times 21 \text{ mm}^2$, and a thickness of 0.5 mm. The base pressure in the chamber is maintained at about 2.0×10^{-8} mbar. At this pressure, a layer of hydrogen, carbon, and oxygen material with a thickness of one molecule would cover the surface in about 1000 s. To reduce the influence of such adsorbates, the target surface was cleaned with the nanoampere ion beam for about 30 min, during which time the target was adjusted slowly in the direction perpendicular to

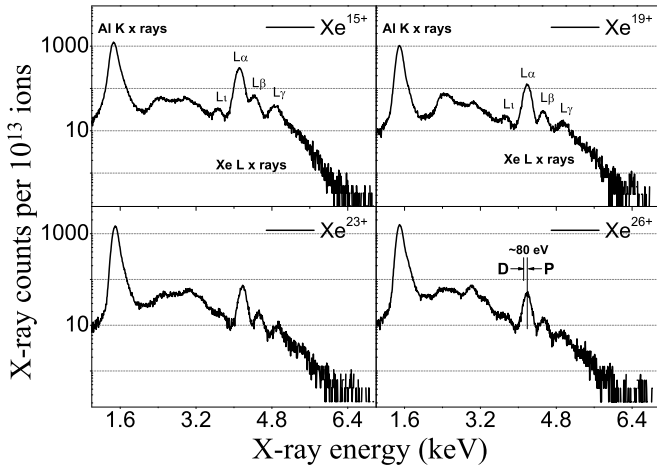


FIG. 2. The measured x-ray spectra for 3480-keV ^{129}Xe ions impinging on the Al target, which consist of the Al K x rays and Xe L x rays. Results are shown for four different initial charge states, $q_{\text{in}} = 15, 19, 23,$ and 26 . For $q_{\text{in}} = 29$, the peak of the measured $L\alpha$ x ray and its diagram line are denoted by P and D, respectively.

the beam, before the x-ray measurements. After transmitting through a 50- μm -thick beryllium window used to seal the vacuum, the emitted x rays are detected by a Si(Li) detector placed at 45° with respect to the beam direction. The total number N_T of incident ions on the target is also measured by using a digital current integrator combined with a timer and counter. The solid angle Ω , seen by the Si(Li) detector from the target, is 23.8 msr, and the energy resolution of the detector is 195 eV at 5.9 keV.

III. RESULTS AND DISCUSSION

Figure 2 shows the measured x-ray spectra from the collisions of 3480-keV ^{129}Xe ions with initial charge state $q_{\text{in}} = 15$ – 26 with the Al target. In order to show the charge-state dependence of the x-ray intensity, the raw x-ray spectra have been normalized to intensity spectra with units per 10^{13} incident ions. The x-ray energies are calibrated by using the characteristic lines radiated from radioisotopes of ^{129}Xe and ^{129}Xe . As shown in Fig. 2, the x-ray spectra consist of Al K - and Xe L -shell characteristic lines. In contrast to the intensity of the Al K -shell x rays, which barely changes with the initial charge state of the projectile, that of the Xe L -shell x rays decreases significantly with an increase of the initial charge state. Moreover, the observed Xe L lines shift toward higher energy by about 80 eV compared to the corresponding diagram lines, which indicates that these x rays are radiated from Xe ions rather than neutral Xe atoms. In addition the charge-state dependence of x-ray lines obtained above, Fig. 3 shows variations of the measured x-ray spectra with the initial kinetic energy of incident ions. The intensity of the Al x rays increases with increasing projectile energy, while non-negligible Xe L x rays are observed only for a projectile energy of 3480 keV.

By assuming an isotropic emission of the x rays, the absolute x-ray yield can be obtained from the x-ray counts, the

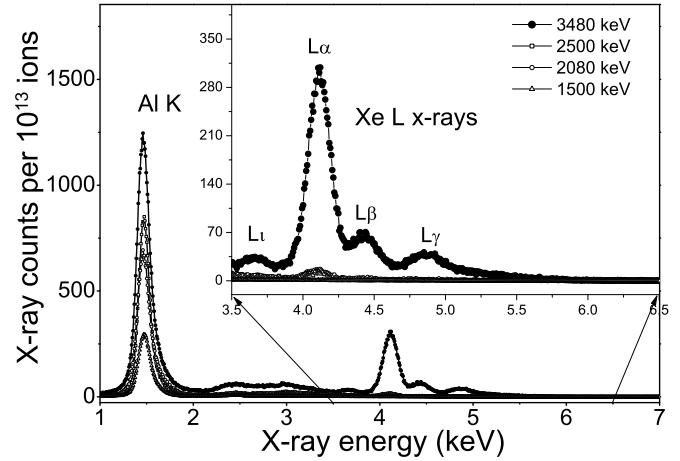


FIG. 3. The measured x-ray spectra for Xe^{15+} ions impinging on the Al target for four different initial kinetic energies, $E_0 = 1500, 2080, 2500,$ and 3480 keV. Non-negligible Xe L x rays are observed only for 3480 keV.

total number of incident ions, the solid angle of the detector seen from the target, the detector efficiency, and the absorptions of 2.0 cm of air and of the 50- μm sealing beryllium window. The obtained yield for the Xe L -shell x rays is shown in Fig. 4(a) as a function of the charge state of the projectile ions. It should be noted that the total number N_P of incident ions is estimated from the measured ion counts N_T on the target using the equation $N_P = N_T / (1 + \gamma / q_{\text{in}})$. A particular value of 2.0 for the quantity γ / q_{in} is estimated with an error of 15% [39–41]. The detection efficiency of the Si(Li) detector

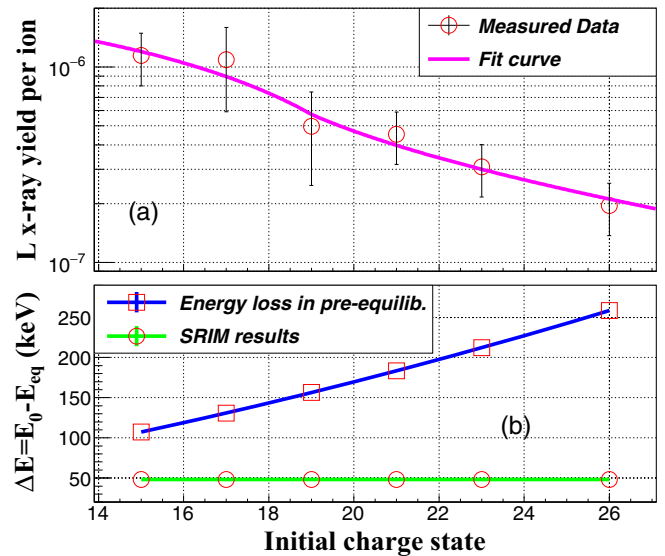


FIG. 4. (a) The measured Xe L -shell x-ray yields for 3480-keV Xe ions with initial charge state q_{in} from 15 to 26 impinging on the Al target. The fit to the measured data with the use of Eqs. (1)–(5) is also plotted. (b) The obtained kinetic energy loss in the course of the pre-equilibration stage, i.e., $\Delta E = E_0 - E_{\text{eq}}$. The SRIM results are also given for comparison.

with a 25- μm beryllium window is 0.92, and the transmission coefficient for the Xe L -shell x rays through the 2 cm of air and 50- μm beryllium window is 0.77 [42]. Since the errors primarily result from uncertainties of the number of incident ions (15%), the observation solid angle (2%), the efficiency of the Si(Li) detector (2%), and the x-ray counting statistics (10%), the overall uncertainty is determined to be about 30%.

Under the assumptions that the Xe ions with initial kinetic energy E_0 and initial charge state q_{in} slow down along a straight trajectory and the associated energy-loss straggling is neglected, the Xe L x-ray yield is given by [2]

$$Y(q_{\text{in}}) = \int_{E_{\text{th}}}^{E_0} \frac{N\sigma_X[E(x)] \times e^{-\mu x}}{S} dE. \quad (1)$$

Here, N represents the number of target atoms per unit volume (60.31 nm $^{-3}$), μ is the x-ray absorption coefficient (7.3 $\times 10^{-5}$ nm $^{-1}$), $\sigma_X[E(x)]$ is the x-ray production cross section at projectile energy $E(x)$, which depends on the depth x of the projectile in the target, and $S = -dE/dx$ is the stopping power of the Al target to the ions. In light of the associated ionization cross section being inversely proportional to the quadratic electron binding energy $U(q_{\text{in}})$ [43] and of the ionization threshold E_{th} being approximately equal to the initial kinetic energy E_0 (see Fig. 3), the x-ray production cross section $\sigma_X[E(R)]$ can be simply expressed as $\sigma_0/U^2(q_{\text{in}})$, where σ_0 is a constant parameter. It should be noted that the assumptions made here are not applicable to the target K x rays anymore since the ionization threshold of the target K -shell electrons is far less than the initial kinetic energy E_0 (see Fig. 3). A detailed analysis of the target x-ray yield is presented in the Appendix.

When Xe ions with initial charge state q_{in} enter into the target, an equilibration charge state q_{eq} will be established after the ions travel an equilibration distance d . According to the linear-response mechanism proposed by Bohr and Lindhard [14] and applied by Brandt *et al.* [19,23,24,27], the charge state q of the projectile at the depth x in the target is given by

$$q(x) = q_{\text{in}} e^{-x/d}. \quad (2)$$

In the preequilibration region, the energy loss will be enhanced by the increase of the ion charge state [16–20], and the stopping power S (consisting of both the electronic stopping and nuclear stopping) is a function of the projectile charge state [15,44]. In the near-Bohr-velocity collisions of highly charged ions, several effects, such as screening of projectile nuclei, the orbital motion of target electrons, and charge exchange, should be taken into account in order to obtain a reasonable stopping power [45]. For simplicity, we assume a power-law dependence of S on q [16,30],

$$S(q_{\text{in}}) = S_{\text{eq}} \left(\frac{q}{q_{\text{eq}}} \right)^n = S_{\text{eq}} \left(\frac{q_{\text{in}}}{q_{\text{eq}}} \right)^n e^{-nx/d}. \quad (3)$$

Here, S_{eq} represents the stopping power after the charge-state equilibrium. Since the ionization threshold E_{th} is close to E_0 (see Fig. 3), we assume S_{eq} is independent of the projectile energy over the integration interval in Eq. (1).

In order to calculate the x-ray yield using Eqs. (1)–(3), the kinetic energy E of the projectile must be known as a function of the depth x . In the case that the projectile kinetic energy E_{eq} at equilibration is less than E_{th} (i.e., $E_{\text{eq}} < E_{\text{th}}$), the kinetic energy E at the depth x is given by

$$\begin{aligned} E(x) &= E_0 - \int_0^x S dx \\ &= E_0 - S_{\text{eq}} \left(\frac{q_{\text{in}}}{q_{\text{eq}}} \right)^n \left(\frac{d}{n} \right) (1 - e^{-nx/d}). \end{aligned} \quad (4)$$

Moreover, in the case of $E_{\text{eq}} > E_{\text{th}}$ [see Fig. 1(b)], for $x < d$ the kinetic energy is identical to Eq. (4), while for $x > d$ it reads

$$\begin{aligned} E(x) &= E_0 - \int_0^d S dx - \int_d^x S dx \\ &= E_0 - S_{\text{eq}} \left(\frac{q_{\text{in}}}{q_{\text{eq}}} \right)^n \left(\frac{d}{n} \right) (1 - e^{-n}) - S_{\text{eq}}(x - d). \end{aligned} \quad (5)$$

Here, $q_{\text{eq}} = 5.88$, which is calculated by means of Eqs. (3) and (4) in Ref. [22], and $S_{\text{eq}} = 3.06$ keV/nm [46]. $U(q_{\text{in}})$ is a weighted mean value of the binding energies of the three L subshells, which are calculated using the GRASP2K package [47]. The weighted binding energies of Xe ions with initial charge states $q_{\text{in}} = 15$ –26 are then fitted with a binomial function, which is sufficient to describe the variation of the weighted binding energies. Hence, for a given power n in Eq. (3), it is possible to calculate the x-ray yield by fitting the three parameters σ_0 , d , and E_{th} by means of Eqs. (1)–(5). The fitting is done using the χ^2 method, and the associated integration is performed with the 51-point Gauss-Kronrod algorithm in the frame of the ROOT package [48]. After testing all of the powers from 1.0 to 2.0 in increments of 0.1, the obtained best-fit parameters for our experimental data are $\sigma_0 = (1.89 \pm 0.30) \times 10^{-2}$ nm 2 eV 2 , $d = 15.72 \pm 1.33$ nm, and $E_{\text{th}} = (3.32 \pm 0.01) \times 10^3$ keV, which correspond to the power $n = 1.6$. The fitting results for other powers are presented in the Appendix. The obtained E_{th} is close to E_0 , which justifies the assumptions made above. It should be noted that since the charge-equilibration length d of ions is slightly different for different initial charge states, the value of d obtained here is an average over those for all the initial charge states used in the present experiment.

By inserting the fitted value of σ_0 into $\sigma_X = \sigma_0/U^2$, the obtained σ_X can be compared with the L -shell x-ray emission cross section deduced from the L -subshell ionization cross sections, which are obtained using the empirical formula of the binary-encounter-approximation theory [43,49]. Actually, a reasonable agreement is achieved (see the Appendix). For instance, for the case of Xe ions with $q_{\text{in}} = 26$ a value of ~ 5.4 barns is obtained from $\sigma_X = \sigma_0/U^2$, in contrast to ~ 6.4 barns from the ionization cross sections. This indicates that the assumptions about σ_X made in Eq. (1) are workable.

With the use of the obtained equilibration length d , we calculated ion kinetic energy E_{eq} at charge equilibration and the resulting energy loss $E_0 - E_{\text{eq}}$ in the course of preequilibration by means of Eq. (4). As can be seen from Fig. 4(b), the obtained energy loss is enhanced by 60–210 keV compared to the SRIM results and increases quickly with an increase of the

initial charge state of Xe ions. Such remarkable enhancements indicate that for collisions of highly charged ions with solids the stopping power cannot be described simply in terms of an equilibration charge state at the beginning of the collisions and that the decrease in the measured x-ray yield is due to the quick loss of ion kinetic energy with an increase of the initial charge state q_{in} . Moreover, it is found that for Xe ions with initial charge state $q_{\text{in}} = 15$ –19 the associated kinetic energy E_{eq} is larger than the fitted E_{th} , whereas for those ions with $q_{\text{in}} = 21$ –26 it becomes smaller. This is why a “knee point” appears at the initial charge state $q_{\text{in}} = 19$ in the fitted curve of Fig. 4(a). In spite of the difference between the values of E_{eq} and E_{th} , they are close roughly to each other for all the initial charge states considered. This reveals that the L x rays of the projectile are emitted primarily in the stage of preequilibration.

The equilibrium time deduced from the fitted equilibrium length d is ~ 6.9 fs, which corresponds to a rate of $\sim 1.5 \times 10^{14} \text{ s}^{-1}$. Note that a shorter equilibration time (~ 2.5 fs) can be obtained by using Bohr’s formula for the equilibration charge state [21]. The present results obtained by measuring the x-ray yields are very consistent with those obtained from the ion-transmission thin-foil experiments (3–7 fs) [19,24,26,27]. In order to interpret such an ultrafast process, new insights have been made in this research field in terms of the interatomic Coulombic decay (ICD) [26], which is essentially different from the previous explanation that the ultrafast deexcitation is due to multiple transition cascades proceeding in parallel. Actually, the ICD occurs following the formation of a screening electron cloud upon impinging of highly charged ions on a solid surface (i.e., so-called hollow atoms [11–13,50]), and the formation rate of the screening cloud depends on the electronic properties of target materials [17,19]. As pointed out in Ref. [16] for slow collisions, the charge-state-dependent energy-loss enhancement may stem from the buildup of the screening cloud around the projectile since collisions with impact parameters comparable to the radii of unoccupied levels of hollow atoms would increase momentum transfers to target electrons and nuclei. By increasing the collision velocity to, for instance, near-Bohr velocity in the present Xe + Al collision system ($E_{\text{th}} = 3320$ keV, corresponding to 1.01 times the Bohr velocity), the ionization of inner-shell electrons of the projectile starts contributing to the energy dissipation of the projectile ions. In addition, surface plasma oscillation induced by the projectile ions [51] may also enhance stopping power near surfaces compared to bulk layers.

IV. CONCLUSION

In summary, we proposed and demonstrated the possibility that the energy loss and equilibration time of highly charged ions traveling through solids can be obtained by measuring the dependence of the x-ray yield on the initial charge state of incident ions. The present results agree well with those obtained in ion-transmission thin-foil experiments, especially for the charge-equilibration time. Moreover, it was demonstrated for the present Xe + Al collision system that the ionization of inner-shell electrons of the projectile, in addition to collisions with its outer-shell electrons, starts contributing

TABLE I. The calculated binding energies (in eV) of the L_i ($i = 1$ –3) subshells of Xe ions with an initial charge state q_{in} from 15 to 26.

q_{in}	$L_1 (2s_{1/2})$	$L_2 (2p_{1/2})$	$L_3 (2p_{3/2})$	Weighted mean values $U(q_{\text{in}})$
15	5936.0	5587.6	5260.8	5511.3
17	5948.1	5598.0	5271.5	5522.2
19	6016.3	5667.3	5340.8	5591.3
21	6104.9	5756.4	5429.6	5680.1
23	6197.3	5849.2	5522.3	5772.8
26	6342.9	5996.0	5668.6	5919.0

to the ion energy loss with an increase of the collision velocity to near-Bohr velocity.

ACKNOWLEDGMENTS

This work is supported by the National Natural Science Foundation of China under Grants No. 12075291, No. 11675279, No. U1732269, No. 11005133, and No. 12174315. We would like to thank the staff of the 320-kV platform for their arrangement and operation of the ECR ion source. We are also very grateful to Dr. Y. J. Yuan and Dr. B. Najjari for their careful revision of the manuscript.

APPENDIX: PROJECTILE L X-RAY CROSS SECTION AND TARGET K X-RAY YIELD

1. Calculation of Xe L -shell binding energies

In the present work, the required binding energies of the L subshells $2s_{1/2}$, $2p_{1/2}$, and $2p_{3/2}$ are calculated using the GRASP2K package [47], which was developed based on the multiconfigurational Dirac-Hartree-Fock method [52]. In the calculations, the single-configuration approximation is adopted, and thus, the ground-state configurations [Ar] $3d^{10}4s^24p^65s^24d$, [Ar] $3d^{10}4s^24p^65s$, [Ar] $3d^{10}4s^24p^5$, [Ar] $3d^{10}4s^24p^3$, [Ar] $3d^{10}4s^24p$, and [Ar] $3d^{10}$ are employed for Xe $^{q_{\text{in}}+}$ ($q_{\text{in}} = 15, 17, 19, 21, 23$, and 26) ions, respectively. The obtained binding energies are listed in Table I together with the weighted mean values $U(q_{\text{in}})$ over the three subshells for reference.

2. L -shell x-ray cross section of Xe

In Sec. III, the Xe L x-ray cross section is assumed to be $\sigma_0/U^2(q_{\text{in}})$. Here, σ_0 is a constant parameter, and $U(q_{\text{in}})$ denotes the weighted mean value. In order to evaluate the reliability of this assumption, the Xe L x-ray cross section σ_L^X is calculated from the L_i -subshell ionization cross sections σ_{L_i} as follows:

$$\sigma_L^X = v_1\sigma_{L_1} + v_2\sigma_{L_2} + v_3\sigma_{L_3}, \quad (\text{A1})$$

where

$$\begin{aligned} v_1 &= \omega_1 + \omega_2 f_{12} + \omega_3 (f_{13} + f_{12} f_{23} + f'_{13}), \\ v_2 &= \omega_2 + \omega_3 f_{23}, \\ v_3 &= \omega_3. \end{aligned} \quad (\text{A2})$$

TABLE II. The fluorescence yields and Coster-Kronig factors for L subshells of Xe.

ω_1	ω_2	ω_3	f_{12}	f_{13}	f_{23}	f'_{23}
0.046	0.083	0.085	0.19	0.28	0.154	4.0×10^{-4}

Here, ω_i are the L_i -subshell fluorescence yields and f_{ij} are the Coster-Kronig factors describing the probabilities of intrashell electron rearrangements. These parameters are taken from Ref. [53], as shown in Table II.

The L_i -subshell ionization cross sections are estimated using the empirical formula derived by McGuire and Richard [43] from the classical binary-encounter-approximation (BEA) theory [49], i.e.,

$$\sigma_{L_i} = (n_{L_i} Z_1^2 \pi e^4) / B_{L_i}^2 G(v), \quad (\text{A3})$$

where $n_{L_1} = n_{L_2} = 2$ and $n_{L_3} = 4$, B_{L_i} is the L_i -subshell binding energy, Z_1 is the nuclear charge of the projectile, and $G(v)$ is a function of the scaled velocity $v = v_1/v_e$, in which v_1 represents the velocity of the projectile and v_e is the orbital velocity of the L_i -subshell electrons.

By inserting Eqs. (A2) and (A3) into Eq. (A1) and using the L -shell binding energies of Xe ions, the corresponding L x-ray cross sections are evaluated and are shown in Table III. Moreover, their counterparts obtained from the fitted parameter σ_0 (see Sec. III) and the weighted mean value $U(q_{\text{in}})$ are also listed in Table III for comparison. As seen clearly, both results agree generally with each other for all the Xe ions, especially for those with higher charge states. This indicates that the fitted σ_0 is reasonable and, further, the approximation made to the L x-ray cross section is feasible.

3. Target K -shell x-ray yield

As shown in Fig. 2, the K x-ray intensity of the Al target barely changes with the initial charge state of the projectile. This indicates that most of the Al K x rays are radiated after the incident highly charged Xe ions have reached the charge-state equilibration. In light of the $\sim 30\%$ experimental error, the charge-state effect on the Al K x rays is hence difficult to observe.

For this reason, the effect of the enhanced stopping power in the preequilibrium region can be neglected, and thus, the K -shell x-ray yield of the Al target can be expressed approximately as

$$Y(E_0) \simeq \int_{E'_{\text{th}}}^{E_0} \frac{N \omega_K \sigma_K(E) \exp(-\mu x)}{S(E)} dE. \quad (\text{A4})$$

TABLE III. Comparison of the L x-ray cross sections (in barns) obtained from the fitted σ_0 and from the BEA theory.

	q_{in}					
	15	17	19	21	23	26
$\sigma_0/U^2(q_{\text{in}})$	6.22	6.20	6.05	5.86	5.67	5.39
BEA theory	8.60	8.53	8.11	7.61	7.13	6.44

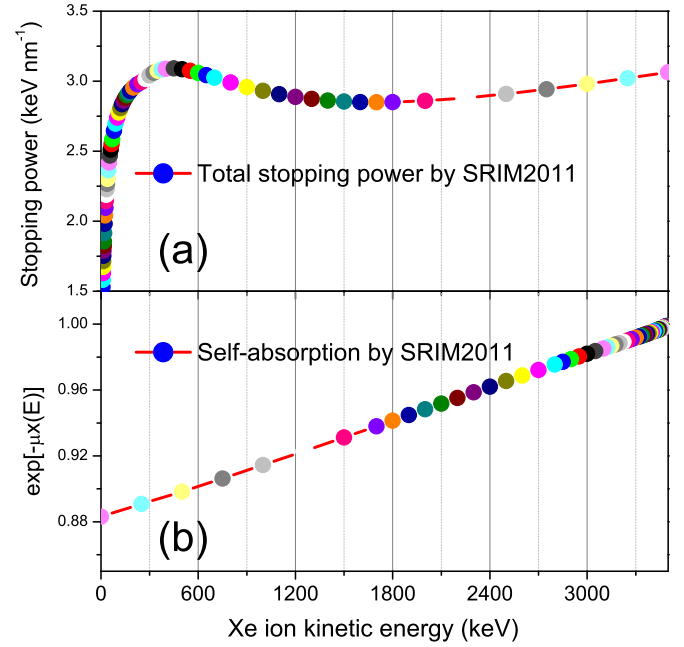


FIG. 5. (a) The stopping power S and (b) the K -shell x-ray self-absorption $\exp(-\mu x)$ as a function of the ion kinetic energy.

Here, $\omega_K = 0.039$ and σ_K denote the Al K -shell fluorescence yield and ionization cross section, respectively. σ_K can be calculated from Eq. (A3). The stopping power S and the K -shell x-ray self-absorption $\exp(-\mu x)$ can be obtained from SRIM [46] and are plotted in Fig. 5 as a function of the ion kinetic energy. Moreover, the threshold energy E'_{th} reads [49,54]

$$E'_{\text{th}} = \frac{B_K}{2} \left(\frac{M_1}{M_2} + 1 \right) \left(\frac{M_1}{m_e Z_1} \right)^{1/2}. \quad (\text{A5})$$

Here, B_K is the K -shell binding energy (1559.6 eV [55]), M_1 and M_2 are the nuclear masses of the projectile

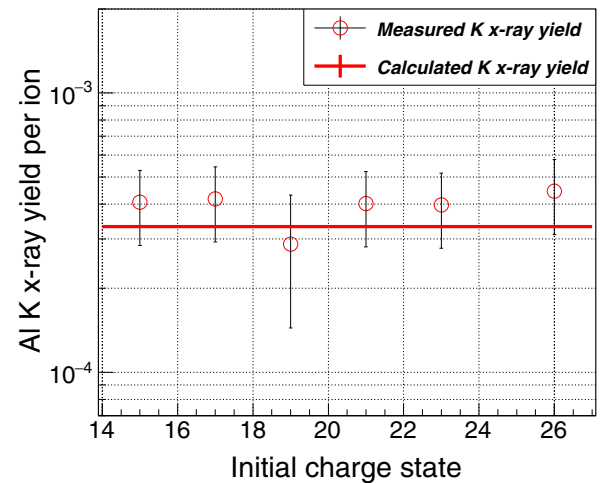


FIG. 6. The measured Al K -shell x-ray yield as a function of the initial charge state of the projectile. The calculated yield from Eq. (A4) is also plotted for comparison.

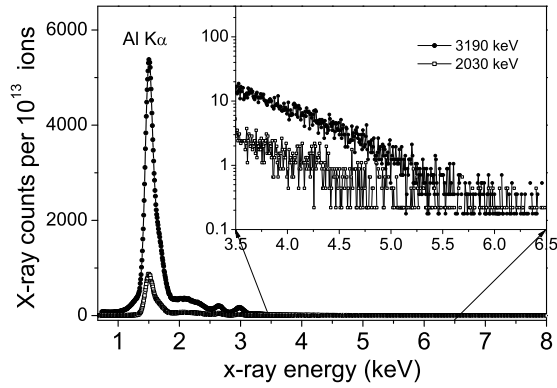


FIG. 7. The measured x-ray spectra from collisions of Xe ions with initial charge state $q_{in} = 29$. No L -shell x rays are observed.

and the target, respectively, and m_e is the electron mass. By using this formula, E'_{th} is determined to be 297.5 keV, which is far less than the initial kinetic energy E_0 (3480 keV) and the charge-equilibrium kinetic energy E_{eq} (about 3320 keV).

Figure 6 shows a comparison of the calculated K -shell x-ray yield from Eq. (A4) with the measured results. The integration is performed using the 51-point Gauss-Kronrod algorithm in the frame of the ROOT program [48]. The use of other algorithms in ROOT produces exactly the same results. As shown in Fig. 6, the calculated results are generally consistent with the experimental ones; the former fall within the experimental uncertainties.

4. L -shell ionization threshold of Xe

As shown in Sec. III, the best fit to the L -shell x-ray yield of Xe ions gives rise to a corresponding ionization energy of about 3320 keV. In the present experiments, although Xe^{29+} ions with initial kinetic energies up to 3190 keV are used to collide with the target, no L -shell x rays of Xe ions are observed, as shown in Fig. 7. Therefore, we be-

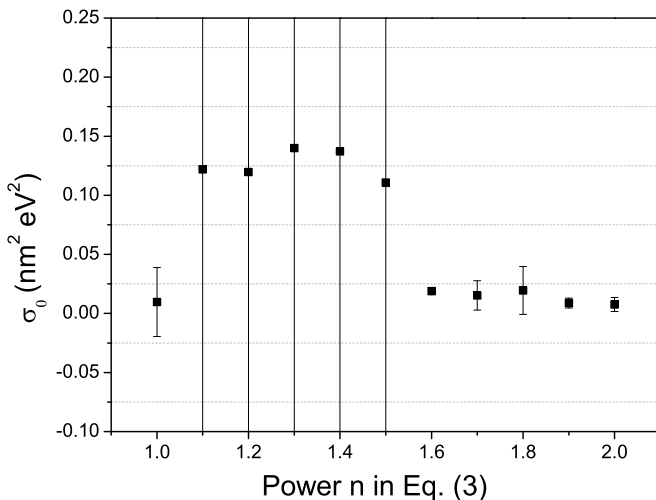


FIG. 8. The fitted σ_0 and its error as a function of the power n ranging from 1.0 to 2.0.

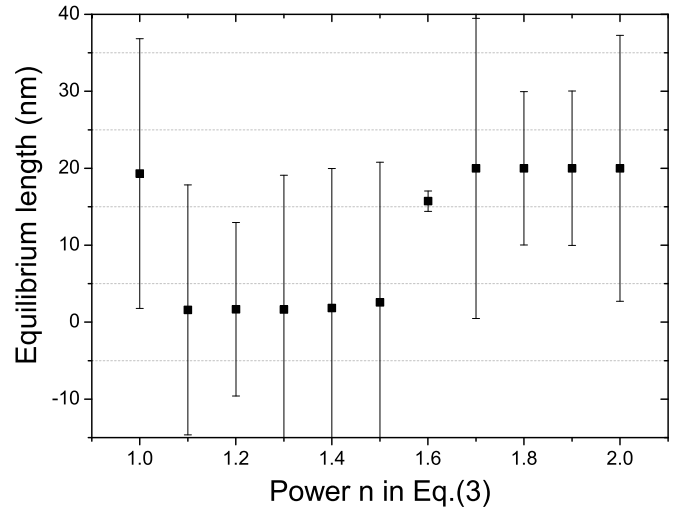


FIG. 9. Same as Fig. 8, but for the equilibrium length d .

lieve that the fitted value of the ionization threshold energy is reliable.

5. Fitting results for other powers n

In Eq. (3), a simple power-law dependence of the preequilibrium stopping power S on the charge state is assumed. The best-fit parameters obtained correspond to the power $n = 1.6$, at which the errors of these parameters are minimum. For other powers between 1.0 and 2.0, the obtained fitting parameters (i.e., σ_0 , equilibrium length d , and ionization threshold E_{th}) are plotted together with their errors in Figs. 8–10, respectively. As is known, the fit errors are related to the initial value and range of the parameters to be fit. In the present work, the initial values of σ_0 , d , and E_{th} are chosen to be $0.025 \text{ nm}^2 \text{ eV}^2$, 4.3 nm, and 3300 keV, respectively, while their respective ranges are $0.002\text{--}1.5 \text{ nm}^2 \text{ eV}^2$, $0.5\text{--}20 \text{ nm}$, and $3100\text{--}3480 \text{ keV}$.

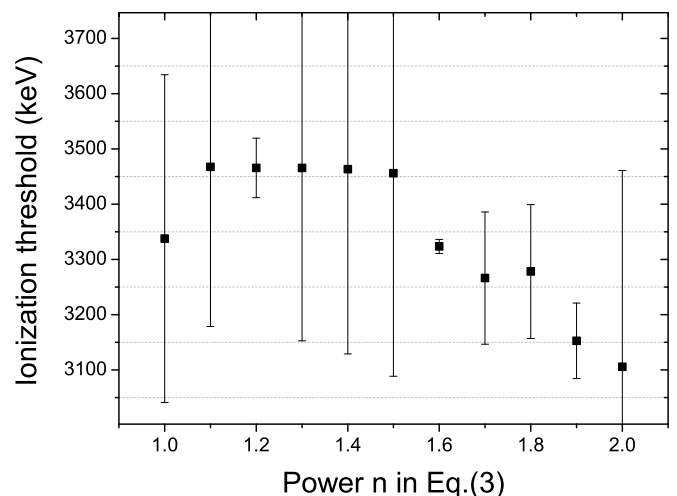


FIG. 10. Same as Fig. 8, but for the ionization threshold E_{th} .

- [1] E. Rutherford, The scattering of α and β particles by matter and the structure of the atom, *London, Edinburgh, Dublin Philos. Mag. J. Sci.* **21**, 669 (1911).
- [2] J. D. Garcia, R. J. Fortner, and T. M. Kavanagh, Inner-Shell Vacancy Production in Ion-Atom Collisions, *Rev. Mod. Phys.* **45**, 111 (1973).
- [3] H. Winter, Collisions of atoms and ions with surfaces under grazing incidence, *Phys. Rep.* **367**, 387 (2002).
- [4] E. Akcöltekin, T. Peters, R. Meyer, A. Duvenbeck, M. Klusmann, I. Monnet, H. Lebius, and M. Schleberger, Creation of multiple nanodots by single ions, *Nat. Nanotechnol.* **2**, 290 (2007).
- [5] R. Heller, S. Facsko, R. A. Wilhelm, and W. Möller, Defect Mediated Desorption of the KBr(001) Surface Induced by Single Highly Charged Ion Impact, *Phys. Rev. Lett.* **101**, 096102 (2008).
- [6] R. A. Wilhelm, A. S. El-Said, F. Krok, R. Heller, E. Gruber, F. Aumayr, and S. Facsko, Highly charged ion induced nanostructures at surfaces by strong electronic excitations, *Prog. Surf. Sci.* **90**, 377 (2015).
- [7] A. S. El-Said, R. A. Wilhelm, R. Heller, M. Sorokin, S. Facsko, and F. Aumayr, Tuning the Fabrication of Nanostructures by Low-Energy Highly Charged Ions, *Phys. Rev. Lett.* **117**, 126101 (2016).
- [8] Y. T. Zhao, Y. N. Zhang, R. Cheng, B. He, C. L. Liu, X. M. Zhou, Y. Lei, Y. Y. Wang, J. R. Ren, X. Wang, Y. H. Chen, G. Q. Xiao, S. M. Savin, R. Gavrilin, A. A. Golubev, and D. H. H. Hoffmann, Benchmark Experiment to Prove the Role of Projectile Excited States upon the Ion Stopping in Plasmas, *Phys. Rev. Lett.* **126**, 115001 (2021).
- [9] J. Ren, Z. Deng, W. Qi, B. Chen, B. Ma, X. Wang, S. Yin, J. Feng, W. Liu, Z. Xu *et al.*, Observation of a high degree of stopping for laser-accelerated intense proton beams in dense ionized matter, *Nat. Commun.* **11**, 5157 (2020).
- [10] D. Schulz-Ertner and H. Tsujii, Particle radiation therapy using proton and heavier ion beams, *J. Clin. Oncol.* **25**, 953 (2007).
- [11] J. P. Briand, L. de Billy, P. Charles, S. Essabaa, P. Briand, R. Geller, J. P. Desclaux, S. Bliman, and C. Ristori, Production of Hollow Atoms by the Excitation of Highly Charged Ions in Interaction with a Metallic Surface, *Phys. Rev. Lett.* **65**, 159 (1990).
- [12] A. Arnau, F. Aumayr, P. M. Echenique, M. Grether, W. Heiland, J. Limburg, R. Morgenstern, P. Roncin, S. Schippers, R. Schuch, N. Stolterfoht, P. Varga, T. J. M. Zouros, and H. P. Winter, Interaction of slow multicharged ions with solid surfaces, *Surf. Sci. Rep.* **27**, 113 (1997).
- [13] T. Schenkel, A. V. Hamza, A. V. Barnes, and D. H. Schneider, Interaction of slow, very highly charged ions with surfaces, *Prog. Surf. Sci.* **61**, 23 (1999).
- [14] N. Bohr and J. Lindhard, XXVIII. Electron capture and loss by heavy ions penetrating through matter, in *Niels Bohr Collected Works* (Bianco Lunos Bogirykkeri A/S, Denmark, 1987), Vol. 8, p. 593.
- [15] C. P. Race, D. R. Mason, M. W. Finnis, W. M. C. Foulkes, A. P. Horsfield, and A. P. Sutton, The treatment of electronic excitations in atomistic models of radiation damage in metals, *Rep. Prog. Phys.* **73**, 116501 (2010).
- [16] T. Schenkel, M. A. Briere, A. V. Barnes, A. V. Hamza, K. Bethge, H. Schmidt-Böcking, and D. H. Schneider, Charge State Dependent Energy Loss of Slow Heavy Ions in Solids, *Phys. Rev. Lett.* **79**, 2030 (1997).
- [17] J. I. Juaristi, A. Arnau, P. M. Echenique, C. Auth, and H. Winter, Charge State Dependence of the Energy Loss of Slow Ions in Metals, *Phys. Rev. Lett.* **82**, 1048 (1999).
- [18] R. A. Wilhelm, E. Gruber, V. Smejkal, S. Facsko, and F. Aumayr, Charge-state-dependent energy loss of slow ions. I. Experimental results on the transmission of highly charged ions, *Phys. Rev. A* **93**, 052708 (2016).
- [19] E. Gruber, R. A. Wilhelm, R. Pétuya, V. Smejkal, R. Kozubek, A. Hierzenberger, B. C. Bayer, I. Aldazabal, A. K. Kazansky, F. Libisch, A. V. Krasheninnikov, M. Schleberger, S. Facsko, A. G. Borisov, A. Arnau, and F. Aumayr, Ultrafast electronic response of graphene to a strong and localized electric field, *Nat. Commun.* **7**, 13948 (2016).
- [20] R. A. Wilhelm and P. L. Grande, Unraveling energy loss processes of low energy heavy ions in 2D materials, *Commun. Phys.* **2**, 89 (2019).
- [21] N. Bohr, XXII. The penetration of atomic particles through matter, in *Niels Bohr Collected Works* (Bianco Lunos Bogirykkeri A/S, Denmark, 1987), Vol. 8, p. 423.
- [22] G. Schiwietz and P. L. Grande, Improved charge-state formulas, *Nucl. Instrum. Methods Phys. Res., Sect. B* **175-177**, 125 (2001).
- [23] W. Brandt, R. Laubert, M. Mourino, and A. Schwarzschild, Dynamic Screening of Projectile Charges in Solids Measured by Target X-Ray Emission, *Phys. Rev. Lett.* **30**, 358 (1973).
- [24] M. Hattass, T. Schenkel, A. V. Hamza, A. V. Barnes, M. W. Newman, J. W. McDonald, T. R. Niedermayr, G. A. Machicoane, and D. H. Schneider, Charge Equilibration Time of Slow, Highly Charged Ions in Solids, *Phys. Rev. Lett.* **82**, 4795 (1999).
- [25] R. A. Wilhelm, E. Gruber, R. Ritter, R. Heller, S. Facsko, and F. Aumayr, Charge Exchange and Energy Loss of Slow Highly Charged Ions in 1 nm Thick Carbon Nanomembranes, *Phys. Rev. Lett.* **112**, 153201 (2014).
- [26] R. A. Wilhelm, E. Gruber, J. Schwestka, R. Kozubek, T. I. Madeira, J. P. Marques, J. Kobus, A. V. Krasheninnikov, M. Schleberger, and F. Aumayr, Interatomic Coulombic Decay: The Mechanism for Rapid Deexcitation of Hollow Atoms, *Phys. Rev. Lett.* **119**, 103401 (2017).
- [27] A. Niggas, S. Creutzburg, J. Schwestka, B. Wockinger, T. Gupta, P. L. Grande, D. Eder, J. P. Marques, B. C. Bayer, F. Aumayr, R. Bennett, and R. A. Wilhelm, Peeling graphite layer by layer reveals the charge exchange dynamics of ions inside a solid, *Commun. Phys.* **4**, 180 (2021).
- [28] R. A. Wilhelm and W. Möller, Charge-state-dependent energy loss of slow ions. II. Statistical atom model, *Phys. Rev. A* **93**, 052709 (2016).
- [29] J. Wang, B. Ding, X. Song, Y. Shi, X. Guo, X. Liu, L. Wang, M. Wei, P. Liu, Y. Liu, B. Hu, J. E. Valdés, V. A. E., L. Chen, Y. Guo, and X. Chen, Nuclear versus electronic energy loss in slow Ar ion scattering on a Cu (100) surface: Experiment and simulations, *Phys. Rev. A* **102**, 012805 (2020).
- [30] P. Ström and D. Primetzhofer, Energy deposition by nonequilibrium charge states of MeV ^{129}Xe in Au, *Phys. Rev. A* **103**, 022803 (2021).
- [31] S. Lohmann and D. Primetzhofer, Disparate Energy Scaling of Trajectory-Dependent Electronic Excitations for Slow Protons and He Ions, *Phys. Rev. Lett.* **124**, 096601 (2020).

- [32] J. M. Pruneda, D. Sánchez-Portal, A. Arnau, J. I. Juaristi, and E. Artacho, Electronic Stopping Power in LiF from First Principles, *Phys. Rev. Lett.* **99**, 235501 (2007).
- [33] X. D. Zhao, F. Mao, S. M. Li, B. S. Li, H. Mao, F. Wang, and F. S. Zhang, First-principles study of semicore electron excitation in the electronic energy loss of ZnO for protons, *Phys. Rev. A* **104**, 032801 (2021).
- [34] A. Ojanperä, A. V. Krasheninnikov, and M. Puska, Electronic stopping power from first-principles calculations with account for core electron excitations and projectile ionization, *Phys. Rev. B* **89**, 035120 (2014).
- [35] R. Ullah, E. Artacho, and A. A. Correa, Core Electrons in the Electronic Stopping of Heavy Ions, *Phys. Rev. Lett.* **121**, 116401 (2018).
- [36] C. W. Lee, J. A. Stewart, R. Dingreville, S. M. Foiles, and A. Schleife, Multiscale simulations of electron and ion dynamics in self-irradiated silicon, *Phys. Rev. B* **102**, 024107 (2020).
- [37] L. T. Sun, J. Y. Li, X. Z. Zhang, H. Wang, B. H. Ma, X. X. Li, Y. C. Feng, M. T. Song, Y. H. Zhu, P. Z. Wang, H. P. Liu, H. W. Zhao, X. W. Ma, and W. L. Zhan, Commissioning test of LAPECR2 source on the 320-kV HV platform, *Chin. Phys. C* **31**, 55 (2007).
- [38] Z. Y. Song, Z. H. Yang, G. Q. Xiao, Q. M. Xu, J. Chen, B. Yang, and Z. R. Yang, Charge state effect on K-shell ionization of aluminum by 600-3400 keV Xe^{q+} ($q=12-29$) ion collisions, *Eur. Phys. J. D* **64**, 197 (2011).
- [39] F. Aumayr, H. Kurz, D. Schneider, M. A. Briere, J. W. McDonald, C. E. Cunningham, and H. P. Winter, Emission of Electrons from a Clean Gold Surface Induced by Slow, Very Highly Charged Ions at the Image Charge Acceleration Limit, *Phys. Rev. Lett.* **71**, 1943 (1993).
- [40] J. Krása, L. Láska, M. P. Stöckli, and C. W. Fehrenbach, Electron yield from Be-Cu induced by highly charged Xe^{q+} ions, *Nucl. Instrum. Methods Phys. Res., Sect. B* **196**, 61 (2002).
- [41] Z. Y. Song, Z. H. Yang, H. Q. Zhang, J. X. Shao, Y. Cui, Y. P. Zhang, X. A. Zhang, Y. T. Zhao, X. M. Chen, and G. Q. Xiao, Rydberg-to-M-shell x-ray emission of hollow Xe^{q+} ($q = 27-30$) atoms or ions above metallic surfaces, *Phys. Rev. A* **91**, 042707 (2015).
- [42] J. H. Hubbell and S. M. Seltzer, X-ray mass attenuation coefficients, <http://www.nist.gov/pml/data/xraycoef/>.
- [43] J. H. McGuire and P. Richard, Procedure for computing cross sections for single and multiple ionization of atoms in the Binary-encounter approximation by the impact of heavy charged particles, *Phys. Rev. A* **8**, 1374 (1973).
- [44] J. P. Biersack, The effect of high charge states on the stopping and ranges of ions in solids, *Nucl. Instrum. Methods Phys. Res., Sect. B* **80-81**, 12 (1993).
- [45] P. Sigmund and A. Schinner, Progress in understanding heavy-ion stopping, *Nucl. Instrum. Methods Phys. Res., Sect. B* **382**, 15 (2016).
- [46] J. F. Ziegler, M. D. Ziegler, and J. P. Biersack, SRIM – The stopping and range of ions in matter (2010), *Nucl. Instrum. Methods Phys. Res., Sect. B* **268**, 1818 (2010).
- [47] P. Jönsson, X. He, C. F. Fischer, and I. P. Grant, The grasp2K relativistic atomic structure package, *Comput. Phys. Commun.* **177**, 597 (2007).
- [48] ROOT, <https://root.cern/releases/release-60604/>.
- [49] M. Gryzinski, Classical theory of atomic collisions. I. Theory of inelastic collisions, *Phys. Rev.* **138**, A336 (1965).
- [50] J. Burgdörfer, P. Lerner, and F. W. Meyer, Above-surface neutralization of highly charged ions: The classical over-the-barrier model, *Phys. Rev. A* **44**, 5674 (1991).
- [51] A. Kononov and A. Schleife, Pre-equilibrium stopping and charge capture in proton-irradiated aluminum sheets, *Phys. Rev. B* **102**, 165401 (2020).
- [52] I. P. Grant, *Relativistic Quantum Theory of Atoms and Molecules: Theory and Computation* (Springer, New York, 2007).
- [53] J. L. Campbell, Fluorescence yields and Coster Kronig probabilities for the atomic L subshells, *At. Data Nucl. Data Tables* **85**, 291 (2003).
- [54] H. Zhang, X. Chen, Z. Yang, J. Xu, Y. Cui, J. Shao, X. Zhang, Y. Zhao, Y. Zhang, and G. Xiao, Molybdenum L-shell X-ray production by 350–600 keV Xe^{q+} ($q=25-30$) ions, *Nucl. Instrum. Methods Phys. Res., Sect. B* **268**, 1564 (2010).
- [55] Center for X-ray Optics and Advanced Light Source, Lawrence Berkeley National Laboratory, X-ray data booklet, <http://xdb.lbl.gov/>.